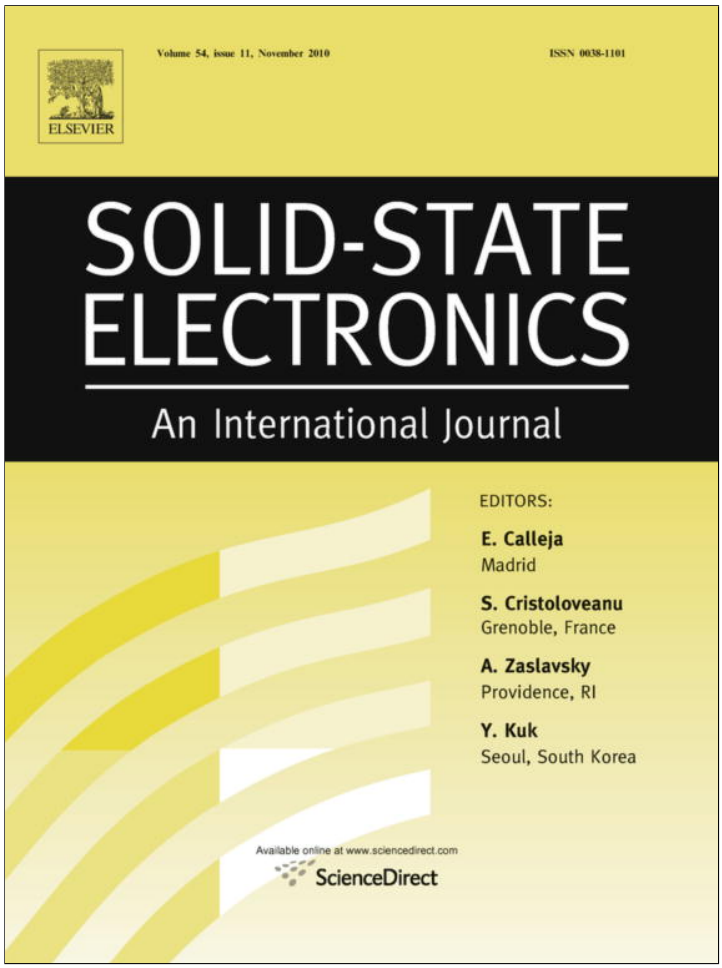

Solid-State Electronics 54 (2010) 1421–1429

Contents lists available at ScienceDirect

Solid-State Electronics

journal homepage: www.elsevier.com/locate/sse

Unified large and small signal non-quasi-static model for long channel symmetric DG MOSFET

Sudipta Sarkar [a,*], Ananda S. Roy [b], Santanu Mahapatra [a]

[a] Nanoscale Device Research Laboratory, Centre for Electronics Design and Technology, Indian Institute of Science, Bangalore 560 012, India
[b] Intel Corporation, Hillsboro, USA

ARTICLE INFO

Article history:
Received 24 February 2010
Received in revised form 21 May 2010
Accepted 25 May 2010
Available online 19 June 2010
The review of this paper was arranged by Prof. A. Zaslavsky

Keywords:
Non-quasi-static (NQS)
Double gate (DG)
Large signal
Small signal
Compact modeling

ABSTRACT

We propose a unified model for large signal and small signal non-quasi-static analysis of long channel symmetric double gate MOSFET. The model is physics based and relies only on the very basic approximation needed for a charge-based model. It is based on the EKV formalism [Enz C, Vittoz EA. Charge based MOS transistor modeling. Wiley; 2006] and is valid in all regions of operation and thus suitable for RF circuit design. Proposed model is verified with professional numerical device simulator and excellent agreement is found.

1. Introduction

Double gate metal oxide semiconductor field effect transistor (DG MOSFET) is appearing as replacement for bulk MOSFET in sub-45 nm technology nodes. In order to use these devices in RF circuit design, one needs to develop efficient models suitable for high frequency operation which will take into account the non-quasi-static effects [1–4]. At these frequencies, the basic assumption of quasi-static (QS) analysis [5] that the channel charge is exclusive function of terminal voltages, breaks down due to the finite transit time of the carriers through the channel, and thus they become unreliable for circuit design purpose. The existing literature [5–9] on symmetric double gate MOSFET is based on quasi-static assumption. To the best of our knowledge, for the first time a unified large- and small-signal NQS model for symmetric DG is being proposed in this work, some initial results of which were presented in [1]. The current equation for a MOSFET (as well as DG MOSFET) can be written as [10],

$$I = -W\mu_n \frac{dV_{ch}}{dx} Q_i \tag{1}$$

and the continuity equation is [10],

$$\frac{\partial I}{\partial x} = W \frac{\partial Q_i}{\partial t} \tag{2}$$

where the I, Q_i, V_{ch}, μ_n, W, t and x denote current, inversion charge, channel quasi-fermi potential, electron mobility, gate width, time and longitudinal direction, respectively. Now if the first equation is substituted in the second one and $\frac{dV_{ch}}{dx}$ is expressed as some function of $\frac{dQ_i}{dx}$, (for detailed description, please refer to Section 3.1) we get a non-linear partial differential equation (PDE) where the dependent variable is the inversion charge Q_i and the independent variables are x and t. Large signal NQS modeling demands an analytical solution of this PDE, which is extremely difficult. Relaxation time based methods [11] are easy to implement but not sufficiently accurate at high frequencies. Channel segmentation methods [12] allow arbitrary level of accuracy but are computationally expensive. Recently effort has been put to solve the PDE directly in a semi-numerical manner. Galerkin [13] and cubic spline method [14] fall in this category. In this paper, we convert the non-linear PDE into ordinary differential equations (ODE) using cubic-spline collocation method developed in [14]. This ODE system is solvable in a circuit simulator as has been shown in [15]. It is useful to mention here that no analytical solution exists till today even for transient non-quasi-static analysis for bulk MOSFET.

However if we are interested in the special case of small signal sinusoidal voltages, then $\frac{\partial}{\partial t}$ can be replaced by $j\omega$ and consequently the problem reduces to an ODE which is solvable analytically. Thus it is possible to obtain analytical expressions for y parameters.

* Corresponding author. Tel.: +91 80 22933090; fax: +91 80 23600808.
E-mail addresses: ssudip@cedt.iisc.ernet.in (S. Sarkar), ananda.s.roy@intel.com (A.S. Roy), santanu@cedt.iisc.ernet.in (S. Mahapatra).

0038-1101/$ - see front matter © 2010 Elsevier Ltd. All rights reserved.
doi:10.1016/j.sse.2010.05.036

Though there are several core models for symmetric DG MOSFET, we have used the EKV model [16] for deriving the NQS parameters. This is because we feel that the EKV model is much simpler compared to the other models for DG, and gives a very simple DC charge control equation. Furthermore, a short channel DC model for symmetric DG [6] has already been proposed by the EKV group which we would like to use in future in order take into consideration the short channel effects in the non-quasi-static analysis. The proposed non-quasi-static model is verified against the numerical device simulator Atlas [17] and excellent agreement is found.

The remainder of the paper is organized as follows. In Section 2, we go through the DC model of symmetric DG MOSFET, in Section 3, we derive the large signal NQS model, in Section 4 we derive the small-signal NQS parameters and finally in Section 5 we validate our model against a professional numerical device simulator.

2. EKV core model of long channel symmetrical DG MOSFET

We assume long channel DG undoped body MOSFET and constant mobility along the channel. Solving the Poisson's equation for the structure shown in Fig. 1 with gradual channel approximation we get [16],

$$V_G - V_{ch} \approx \frac{Q_G}{C_{ox}} + U_T \cdot \ln\left(\frac{Q_G^2}{2 \cdot \epsilon_{si} \cdot e \cdot U_T \cdot n_i} + \frac{Q_G}{e \cdot n_i \cdot t_{si}/2}\right) \tag{3}$$

where Q_G is the charge density per unit area under each gate, e the electronic charge, ϵ_{si} the permittivity of silicon, $U_T(=KT/e)$ the thermal voltage, n_i the intrinsic carrier concentration, t_{si} the silicon film thickness, C_{ox} the oxide capacitance per unit area and V_G is the voltage applied to both the gate electrodes simultaneously. A midgap work function metal gate with a zero barrier with respect to intrinsic silicon has been assumed without loss of generality. Now we introduce a normalization of the channel charge and current according to the EKV model. Note that here the normalization factors are twice that of bulk MOSFETs. Introducing the charge normalization factor $Q_n = -4C_{ox}U_T$ (note the minus sign, it is different from the normalization factor used in [16], but conforms with the sign convention used in [18]) and voltage normalization factor as $V_n = U_T$, (3) can be rewritten as,[1]

$$v_g - v_{ch} + \ln\left(\frac{q_{int}}{2}\right) = 2q_0 + \ln\left(\frac{q_0}{2}\right) + \ln\left(1 + \frac{q_0}{2}\frac{C_{ox}}{C_{si}}\right) \tag{4}$$

where $q_{int} = -e \cdot n_i \cdot t_{si}/Q_n$, $C_{ox} = \frac{\epsilon_{ox}}{t_{ox}}$ and $C_{si} = \frac{\epsilon_{si}}{t_{si}}$, $q_0(=-q_g/2)$ is the normalized inversion charge per unit area. We have neglected any fixed oxide charges. A methodology to compute the mobile charge density as an explicit function of bias voltages (v_g and v_d or v_s) by solving (4) is given in [19]. Taking differential of (4) we get,

$$-dv_{ch} = \left(2 + \frac{1}{q_0} + \frac{\frac{C_{ox}}{2C_{si}}}{1 + \frac{q_0 C_{ox}}{2C_{si}}}\right) dq_0 \tag{5}$$

By substituting $I_0 = i_0 \cdot 4C_{ox}U_T^2 \frac{W}{L}\mu_n$, $Q_0 = -q_0 \cdot 4C_{ox}U_T$ and $x = L \cdot \xi$ (L is the gate length) in the current Eq. (1) with DC conditions, we get

$$i_0 = q_0 \frac{dv_{ch}}{d\xi} \tag{6}$$

From (5) and (6) we get,

$$i_0 = -\left(2q_0 + 1 + \frac{\frac{q_0 C_{ox}}{2C_{si}}}{1 + \frac{q_0 C_{ox}}{2C_{si}}}\right)\frac{dq_0}{d\xi} \tag{7}$$

[1] We use capitalized letters for un-normalized quantities, small letters for normalized quantities, subscript 0 (e.g. q_0) for DC, subscript i (e.g. q_i) for total and $\bar{*}$ (e.g. $\bar{q}$) for small signal quantities. Furthermore, $q_{is(id)}$ represents the total source (drain) charge, $q_{s(d)}$ stands for the DC source (drain) charge and $\overline{q_{s(d)}}$ means small signal source (drain) charge.

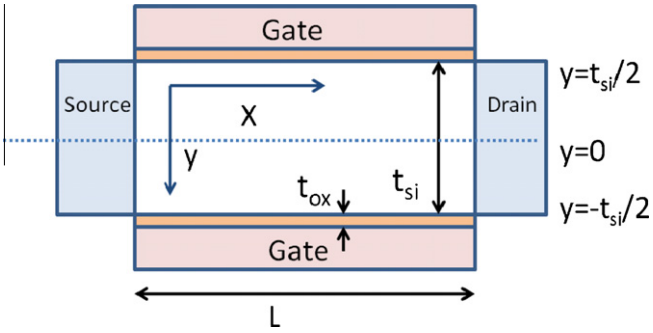

Fig. 1. Schematic of the DG MOSFET structure.

Remembering that DC current is invariant along the transistor length, we integrate from source to drain and get,

$$i_0 \int_0^1 d\xi = \int_{q_d}^{q_s} \left(2q_0 + 1 + \frac{\frac{q_0 C_{ox}}{2C_{si}}}{1 + \frac{q_0 C_{ox}}{2C_{si}}}\right) dq_0 \tag{8}$$

Carrying out the integration we finally obtain,

$$i_0 = L(q_s) - L(q_d) \tag{9}$$

where

$$L(q_0) = q_0^2 + 2q_0 - \frac{2C_{si}}{C_{ox}} \ln\left(1 + \frac{q_0 C_{ox}}{2C_{si}}\right) \tag{10}$$

which can be approximated as,

$$L(q_0) \approx q_0^2 + 2q_0 \tag{11}$$

It is worth mentioning here that Eqs. (3)–(7) are also valid under non steady-state conditions.

3. Large signal non-quasi-static analysis

3.1. Problem formulation

The total current under transient conditions can be expressed as (we replace q_0 and i_0 in (7) with q_i and i),

$$i = -\left(2q_i + 1 + \frac{\frac{q_i C_{ox}}{2C_{si}}}{1 + \frac{q_i C_{ox}}{2C_{si}}}\right)\frac{dq_i}{d\xi} \tag{12}$$

By substitution of $Q_i = -q_i \cdot 4C_{ox}U_T$, $I = i \cdot I_{spec}$, $I_{spec} = 4\mu_n C_{ox} U_T^2 \frac{W}{L}$, $t = \frac{\tau}{\omega_0}$ and $\omega_0 = \frac{\mu_n U_T}{L^2}$ in the continuity Eq. (2) we obtain,

$$\frac{\partial i}{\partial \xi} = -\frac{\partial q_i}{\partial \tau} \tag{13}$$

where every quantity is normalized. Using (12) in (13), we get,

$$\frac{\partial}{\partial \xi}\left[\left(2q_i + 1 + \frac{\frac{q_i C_{ox}}{2C_{si}}}{1 + \frac{q_i C_{ox}}{2C_{si}}}\right)\frac{\partial q_i}{\partial \xi}\right] = \frac{\partial q_i}{\partial \tau} \tag{14}$$

It should be noted that there is no non-quasi-static effect in the inversion charge at source and drain terminals, so $q_i(0,\tau) = q_{is}(\tau)$ and $q_i(1,\tau) = q_{id}(\tau)$ are computed by solving (4) at the source and drain. These are the boundary conditions of the PDE (14). We recall from (9), $i_0 = L(q_s) - L(q_d)$. If the integration is done from source to ξ in (8), we get, $i_0\xi = L(q_s) - L(q_i(\xi))$. Hence,

$$\xi = \frac{L(q_s) - L(q_i(\xi))}{L(q_s) - L(q_d)} \tag{15}$$

Carrying out the simplification, we have,

$$q_i(\xi, \tau = 0) = -1 + \sqrt{1 + L(q_s) - \xi(L(q_s) - L(q_d))} \tag{16}$$

which is the initial condition of the PDE given in (14). Please note that the initial condition has to be calculated at steady state, because (16) is true for DC conditions only.

3.2. Solution by cubic-spline collocation method

Now we shall use the method developed in [14] to derive a semi-numerical solution for the non-linear PDE developed above. We divide the channel into three regions, $0 \leqslant \xi \leqslant \frac{1}{3}$, $\frac{1}{3} \leqslant \xi \leqslant \frac{2}{3}$ and $\frac{2}{3} \leqslant \xi \leqslant 1$. Next we use three cubic equations in these three regions to approximate q_i as follows:

$$q_i(\xi) = \begin{cases} a_1 + b_1 \cdot \xi + c_1 \cdot \xi^2 + d_1 \cdot \xi^3 & 0 \leqslant \xi \leqslant \frac{1}{3} \\ a_2 + b_2 \cdot \xi + c_2 \cdot \xi^2 + d_2 \cdot \xi^3 & \frac{1}{3} \leqslant \xi \leqslant \frac{2}{3} \\ a_3 + b_3 \cdot \xi + c_3 \cdot \xi^2 + d_3 \cdot \xi^3 & \frac{2}{3} \leqslant \xi \leqslant 1 \end{cases} \tag{17}$$

The system of Eq. (17) has to satisfy $q_i(0,\tau)$ and $q_i(1,\tau)$ at the boundaries at all τ. Along with that we have the continuity conditions at the region boundaries as follows:

$$\begin{aligned} q_i\left(\frac{1}{3}\right)^- &= q_i\left(\frac{1}{3}\right)^+ = q_i\left(\frac{1}{3}\right) \\ q_i\left(\frac{2}{3}\right)^- &= q_i\left(\frac{2}{3}\right)^+ = q_i\left(\frac{2}{3}\right) \\ \left.\frac{dq_i}{d\xi}\right|_{1/3-} &= \left.\frac{dq_i}{d\xi}\right|_{1/3+} \\ \left.\frac{dq_i}{d\xi}\right|_{2/3-} &= \left.\frac{dq_i}{d\xi}\right|_{2/3+} \\ \left.\frac{d^2q_i}{d\xi^2}\right|_{1/3-} &= \left.\frac{d^2q_i}{d\xi^2}\right|_{1/3+} \\ \left.\frac{d^2q_i}{d\xi^2}\right|_{2/3-} &= \left.\frac{d^2q_i}{d\xi^2}\right|_{2/3+} \end{aligned} \tag{18}$$

Furthermore, we have the natural boundary conditions,

$$\begin{aligned} \left.\frac{d^2q_i}{d\xi^2}\right|_0 &= 0 \\ \left.\frac{d^2q_i}{d\xi^2}\right|_1 &= 0 \end{aligned} \tag{19}$$

Please note here that $q_i(\frac{1}{3},0)$ and $q_i(\frac{2}{3},0)$ are to be calculated from (16). The 12 conditions defined above help us to determine the 12 constants (they are functions of time, but independent of ξ) $a_{1,2,3}$, $b_{1,2,3}$, $c_{1,2,3}$ and $d_{1,2,3}$. Solving the system of equations, we get,

$$\begin{aligned} a_1 &= q_i(0) \\ b_1 &= -\frac{19}{5}q_i(0) + \frac{1}{5}q_i(1) + \frac{24}{5}q_i\left(\frac{1}{3}\right) - \frac{6}{5}q_i\left(\frac{2}{3}\right) \\ c_1 &= 0 \\ d_1 &= -\frac{36}{5}q_i(0) - \frac{9}{5}q_i(1) - \frac{81}{5}q_i\left(\frac{1}{3}\right) + \frac{54}{5}q_i\left(\frac{2}{3}\right) \\ a_2 &= +\frac{8}{5}q_i(0) - \frac{2}{5}q_i(1) - \frac{8}{5}q_i\left(\frac{1}{3}\right) + \frac{7}{5}q_i\left(\frac{2}{3}\right) \\ b_2 &= -\frac{46}{5}q_i(0) + \frac{19}{5}q_i(1) + \frac{96}{5}q_i\left(\frac{1}{3}\right) - \frac{69}{5}q_i\left(\frac{2}{3}\right) \\ c_2 &= \frac{81}{5}q_i(0) - \frac{54}{5}q_i(1) - \frac{216}{5}q_i\left(\frac{1}{3}\right) + \frac{189}{5}q_i\left(\frac{2}{3}\right) \\ d_2 &= -9q_i(0) + 9q_i(1) + 27q_i\left(\frac{1}{3}\right) - 27q_i\left(\frac{2}{3}\right) \\ a_3 &= -\frac{8}{5}q_i(0) + \frac{22}{5}q_i(1) + \frac{48}{5}q_i\left(\frac{1}{3}\right) - \frac{57}{5}q_i\left(\frac{2}{3}\right) \\ b_3 &= \frac{26}{5}q_i(0) - \frac{89}{5}q_i(1) - \frac{156}{5}q_i\left(\frac{1}{3}\right) + \frac{219}{5}q_i\left(\frac{2}{3}\right) \\ c_3 &= -\frac{27}{5}q_i(0) + \frac{108}{5}q_i(1) + \frac{162}{5}q_i\left(\frac{1}{3}\right) - \frac{243}{5}q_i\left(\frac{2}{3}\right) \\ d_3 &= \frac{9}{5}q_i(0) - \frac{36}{5}q_i(1) - \frac{54}{5}q_i\left(\frac{1}{3}\right) + \frac{81}{5}q_i\left(\frac{2}{3}\right) \end{aligned} \tag{20}$$

The key point of this method is that $q_i(\frac{1}{3})$ and $q_i(\frac{2}{3})$ have to satisfy the PDE (14) exactly. We denote $\frac{C_{ox}}{2 \cdot C_{si}} = m$, and after expanding (14) we get,

$$\left(2q_i + 1 + \frac{m \cdot q_i}{1 + m \cdot q_i}\right)\frac{\partial^2 q_i}{\partial \xi^2} + \left(2 + \frac{m}{(1 + m \cdot q_i)^2}\right)\left(\frac{\partial q_i}{\partial \xi}\right)^2 = \frac{\partial q_i}{\partial \tau} \tag{21}$$

Substituting $q = q_i(\frac{1}{3})$ and $q = q_i(\frac{2}{3})$, respectively, in (21) we get (22) and (23),

$$\left[2q_i\left(\frac{1}{3}\right) + 1 + \frac{m \cdot q_i(\frac{1}{3})}{1 + m \cdot q_i(\frac{1}{3})}\right]\left.\frac{\partial^2 q_i}{\partial \xi^2}\right|_{\xi=\frac{1}{3}} + \left[2 + \frac{m}{(1 + m \cdot q_i(\frac{1}{3}))^2}\right]\left.\left(\frac{\partial q_i}{\partial \xi}\right)^2\right|_{\xi=\frac{1}{3}} = \frac{\partial q_i(\frac{1}{3})}{\partial \tau} \tag{22}$$

$$\left[2q_i\left(\frac{2}{3}\right) + 1 + \frac{m \cdot q_i(\frac{2}{3})}{1 + m \cdot q_i(\frac{2}{3})}\right]\left.\frac{\partial^2 q_i}{\partial \xi^2}\right|_{\xi=\frac{2}{3}} + \left[2 + \frac{m}{(1 + m \cdot q_i(\frac{2}{3}))^2}\right]\left.\left(\frac{\partial q_i}{\partial \xi}\right)^2\right|_{\xi=\frac{2}{3}} = \frac{\partial q_i(\frac{2}{3})}{\partial \tau} \tag{23}$$

where

$$\begin{aligned} \left.\frac{\partial q_i}{\partial \xi}\right|_{\xi=\frac{1}{3}} &= -\frac{7}{5}q_i(0) - \frac{2}{5}q_i(1) - \frac{3}{5}q_i\left(\frac{1}{3}\right) + \frac{12}{5}q_i\left(\frac{2}{3}\right) \\ \left.\frac{\partial^2 q_i}{\partial \xi^2}\right|_{\xi=\frac{1}{3}} &= \frac{72}{5}q_i(0) - \frac{18}{5}q_i(1) - \frac{162}{5}q_i\left(\frac{1}{3}\right) + \frac{108}{5}q_i\left(\frac{2}{3}\right) \end{aligned} \tag{24}$$

and,

$$\begin{aligned} \left.\frac{\partial q_i}{\partial \xi}\right|_{\xi=\frac{2}{3}} &= \frac{2}{5}q_i(0) + \frac{7}{5}q_i(1) - \frac{12}{5}q_i\left(\frac{1}{3}\right) + \frac{3}{5}q_i\left(\frac{2}{3}\right) \\ \left.\frac{\partial^2 q_i}{\partial \xi^2}\right|_{\xi=\frac{2}{3}} &= -\frac{18}{5}q_i(0) + \frac{72}{5}q_i(1) + \frac{108}{5}q_i\left(\frac{1}{3}\right) - \frac{162}{5}q_i\left(\frac{2}{3}\right) \end{aligned} \tag{25}$$

Finally, the coupled ordinary differential Eqs. (22) and (23) are solved to calculate $q_i(\frac{1}{3},\tau)$ and $q_i(\frac{2}{3},\tau)$. It is worth mentioning here that these coupled ODEs can be solved as in [21] by selecting appropriate sub-circuits.

3.3. Derivation of terminal currents

From [20] we can write,

$$I_D(t) = I_0(t) + \frac{d}{dt} \cdot \int_0^L W\frac{x}{L}Q_i(x,t)dx \tag{26}$$

where $I_D(t)$ is the total time varying drain current, $I_0(t)$ is the steady state drain current computed from the DC current equation considering time varying voltage. Normalizing it with the usual normalizing factors of the DG EKV Model we get,

$$i_d(\tau) = i_0(\tau) - \frac{d}{d\tau} \cdot \int_0^1 q_i\xi d\xi \tag{27}$$

where small letters denote corresponding normalized quantities. Similarly, we can derive,

$$i_s(\tau) = -\left(i_0(\tau) + \frac{d}{d\tau}\cdot\int_0^1 q_i(1-\xi)d\xi\right) \tag{28}$$

where $i_s(\tau)$ is the normalized total source current entering the source, and hence the leading negative sign. Using the expression for q_i in the three regions, i.e. $0 \leqslant \xi \leqslant \frac{1}{3}$, $\frac{1}{3} \leqslant \xi \leqslant \frac{2}{3}$ and $\frac{2}{3} \leqslant \xi \leqslant 1$ along with the values of $a_1 \ldots d_3$ (20) in (27) and (28) we get the expressions for drain and source current as follows,

$$i_d(\tau) = i_0(\tau) - \frac{d}{d\tau}\cdot\left[\frac{1}{90}q_i(0) + \frac{11}{90}q_i(1) + \frac{1}{10}q_i\left(\frac{1}{3}\right) + \frac{4}{15}q_i\left(\frac{2}{3}\right)\right] \tag{29}$$

$$i_s(\tau) = -i_0(\tau) - \frac{d}{d\tau}\cdot\left[\frac{11}{90}q_i(0) + \frac{1}{90}q_i(1) + \frac{4}{15}q_i\left(\frac{1}{3}\right) + \frac{1}{10}q_i\left(\frac{2}{3}\right)\right] \tag{30}$$

As DG MOSFET is a three terminal device, gate current can be calculated as $i_g(\tau) = -(i_d(\tau) + i_s(\tau))$. To un-normalize the currents, we need to multiply them with I_{spec}.

4. Small signal non-quasi-static analysis

In a generalised charge-based model for DG MOSFET, we can write [18],

$$i(\xi) = f(q_i)\frac{dq_i}{d\xi} \tag{31}$$

where $i(\xi)$ represents the total normalized current and q_i is the total normalized inversion charge per unit area. It is useful to mention here that from (31) we get the DC current equation,

$$i_0 = f(q_0)\frac{dq_0}{d\xi} \tag{32}$$

Now performing the perturbation analysis of (31) we can write

$$i_0 + \overline{i(\xi)} = f(q_0+\bar{q})\frac{d(q_0+\bar{q})}{d\xi} \tag{33}$$

where the overbarred symbols represent small signal quantities. Expanding by Taylor's series we get,

$$i_0 + \overline{i(\xi)} = f(q_0)\frac{dq_0}{d\xi} + f(q_0)\frac{d\bar{q}}{d\xi} + \frac{df}{dq_0}\bar{q}\frac{dq_0}{d\xi} \tag{34}$$

where we have neglected second order effects. So, $\overline{i(\xi)}$ becomes

$$\overline{i(\xi)} = f(q_0)\frac{d\bar{q}}{d\xi} + \frac{df}{d\xi}\bar{q} \tag{35}$$

So finally we obtain

$$\overline{i(\xi)} = \frac{d(f(q_0)\bar{q})}{d\xi} \tag{36}$$

We have already derived the normalized form of the continuity equation in Section 3 as,

$$\frac{\partial i}{\partial \xi} = -\frac{\partial q_i}{\partial \tau} \tag{37}$$

Putting $i = i_0 + \bar{i}$ and $q_i = q_0(\xi) + \overline{q(\xi,\tau)}$ we get (i and q_i are total quantities, i_0 and q_0 are DC quantities, $\bar{i}$ and $\overline{q(\xi,\tau)}$ are small signal quantities),

$$\frac{\partial \bar{i}}{\partial \xi} = -\frac{\partial \overline{q(\xi,\tau)}}{\partial \tau} \tag{38}$$

which is equivalent to

$$\frac{d\bar{i}}{\partial \xi} = -j\omega_n\bar{q} \tag{39}$$

where ω_n is the normalized frequency. Again (32) can be modified to write

$$\frac{d\xi}{dq_0} = \frac{f(q_0)}{i_0} \tag{40}$$

Therefore from (39) and (40) we get,

$$\frac{d\bar{i}}{dq_0} = -j\omega_n\bar{q}\frac{f(q_0)}{i_0} \tag{41}$$

Now, from (36), (41) and (40) we get,

$$\frac{d^2\bar{i}}{dq_0^2} + \frac{j\omega_n}{i_0^2}f(q_0)\bar{i} = 0 \tag{42}$$

From (32) and (7) and approximating $\frac{q_0C_{ox}}{2C_{si}}\Big/\left(1+\frac{q_0C_{ox}}{2C_{si}}\right) \approx 1$ we get,

$$\frac{d^2\bar{i}}{dq_0^2} - 2\frac{j\omega_n}{i_0^2}(q_0+1)\bar{i} = 0 \tag{43}$$

Now let us substitute $q_0 + 1 = x$, $\bar{i} = y$ and $k = -2\frac{j\omega_n}{i_0^2}$. Then (43) becomes

$$\frac{d^2y}{dx^2} + kxy = 0 \tag{44}$$

Then by substitution of $y = u\sqrt{x}$ and $z = \frac{2}{3}\sqrt{k}x^{\frac{3}{2}}$ (44) becomes

$$z^2\frac{d^2u}{dz^2} + z\frac{du}{dz} + \left(z^2 - \frac{1}{9}\right)u = 0 \tag{45}$$

which is nothing but Bessel's differential equation. So we can write the solution in terms of Bessel functions of the first kind with fractional order,

$$u = c_1J_{\frac{1}{3}}(z) + c_2J_{-\frac{1}{3}}(z) \tag{46}$$

In terms of $\bar{i}$ and q_0 the solution is

$$\bar{i} = \sqrt{q_0+1}\left(c_1J_{\frac{1}{3}}(G(q_0)) + c_2J_{-\frac{1}{3}}(G(q_0))\right) \tag{47}$$

where

$$G(q_0) = \left(\frac{2\sqrt{2\omega_n}}{3i_0}e^{\frac{3j\pi}{4}}(q_0+1)^{\frac{3}{2}}\right) \tag{48}$$

We can determine the charge perturbation $\bar{q}$, from (41) by differentiation of (47) as follows:

$$\frac{d\bar{i}}{dq_0} = (q_0+1)\frac{\sqrt{2\omega_n}}{i_0}e^{3j\frac{\pi}{4}}\cdot\left[c_1J_{-\frac{2}{3}}(G(q_0)) - c_2J_{\frac{2}{3}}(G(q_0))\right] \tag{49}$$

where the relations $J_n'(x) + \left(\frac{n}{x}\right)J_n(x) = J_{n-1}(x)$ and $J_n'(x) - \left(\frac{n}{x}\right)J_n(x) = -J_{n+1}(x)$ have been used. Now from (41) we get,

$$\bar{q} = \frac{1}{\sqrt{2\omega_n}}e^{j\frac{\pi}{4}}\left[c_1J_{-\frac{2}{3}}(G(q_0)) - c_2J_{\frac{2}{3}}(G(q_0))\right] \tag{50}$$

In (50) we substitute $[\overline{q_s}, q_s]$ and $[\overline{q_d}, q_d]$ and get the following two equations

$$\overline{q_s} = \frac{1}{\sqrt{2\omega_n}}e^{j\frac{\pi}{4}}\left[c_1J_{-\frac{2}{3}}(G(q_s)) - c_2J_{\frac{2}{3}}(G(q_s))\right] \tag{51}$$

$$\overline{q_d} = \frac{1}{\sqrt{2\omega_n}}e^{j\frac{\pi}{4}}\left[c_1J_{-\frac{2}{3}}(G(q_d)) - c_2J_{\frac{2}{3}}(G(q_d))\right] \tag{52}$$

where $\overline{q_s(d)}$ is the charge perturbation at source (drain) and q_s (d) is the d·c charge at source (drain). From these two equations we can solve for c_1 and c_2 as follows:

$$c_1 = \frac{\sqrt{2\omega_n}e^{-j\frac{\pi}{4}}\left(\overline{q_s}J_{\frac{2}{3}}(G(q_d)) - \overline{q_d}J_{\frac{2}{3}}(G(q_s))\right)}{J_{\frac{2}{3}}(G(q_d))J_{-\frac{2}{3}}(G(q_s)) - J_{\frac{2}{3}}(G(q_s))J_{-\frac{2}{3}}(G(q_d))} \tag{53}$$

$$c_2 = \frac{\sqrt{2\omega_n}e^{-j\frac{\pi}{4}}\left(\overline{q_s}J_{-\frac{2}{3}}(G(q_d)) - \overline{q_d}J_{-\frac{2}{3}}(G(q_s))\right)}{J_{\frac{2}{3}}(G(q_d))J_{-\frac{2}{3}}(G(q_s)) - J_{\frac{2}{3}}(G(q_s))J_{-\frac{2}{3}}(G(q_d))} \tag{54}$$

Now we define the fundamental charge based Y parameters as in [1,2],

$$\overline{i_s} = Y^q_{ss}\overline{q_s} + Y^q_{sd}\overline{q_d} \tag{55}$$

$$\overline{i_d} = Y^q_{ds}\overline{q_s} + Y^q_{dd}\overline{q_d} \tag{56}$$

where $\overline{i_s}(=\overline{i(\xi=0)})$ is the small signal current leaving the device through the source terminal and $\overline{i_d}(=\overline{i(\xi=1)})$ is entering the device through the drain terminal. Substituting the values of c_1 and c_2 in (47) we get the fundamental charge based Y parameters (we are using Y for charge based and y for voltage domain y parameters),

$$Y^q_{s(d)s} = \sqrt{q_{s(d)}+1}\sqrt{2\omega_n}e^{-j\frac{\pi}{4}} \times \frac{J_{\frac{1}{3}}(G(q_{s(d)}))J_{\frac{2}{3}}(G(q_d)) + J_{-\frac{1}{3}}(G(q_{s(d)}))J_{-\frac{2}{3}}(G(q_d))}{J_{\frac{2}{3}}(G(q_d))J_{-\frac{2}{3}}(G(q_s)) - J_{\frac{2}{3}}(G(q_s))J_{-\frac{2}{3}}(G(q_d))} \tag{57}$$

$$Y^q_{s(d)d} = -\sqrt{q_{s(d)}+1}\sqrt{2\omega_n}e^{-j\frac{\pi}{4}} \times \frac{J_{\frac{1}{3}}(G(q_{s(d)}))J_{\frac{2}{3}}(G(q_s)) + J_{-\frac{1}{3}}(G(q_{s(d)}))J_{-\frac{2}{3}}(G(q_s))}{J_{\frac{2}{3}}(G(q_d))J_{-\frac{2}{3}}(G(q_s)) - J_{\frac{2}{3}}(G(q_s))J_{-\frac{2}{3}}(G(q_d))} \tag{58}$$

We see that there is a term (q_0+1) in expressions for charge based Y parameters as well as in $G(q_0)$. This is a direct consequence of the approximation $\frac{C_{ox}\cdot q_0}{2C_{si}}\Big/\left(1+\frac{q_0C_{ox}}{2C_{si}}\right)\approx 1$ while deriving $f(q_0)$. While this approximation allows us to solve the differential equation, it does introduce a small error in weak inversion where this term is almost zero instead of 1. So $f(q_0)\approx -2(q_0+0.5)$ in weak inversion whereas in strong inversion it is approximately $-2(q_0+1)$. To take care of this, we change the term (q_0+1) in the expressions for $G(q_0)$ and charge based Y parameters to $q_0+\frac{1}{2}+\frac{1}{2}\cdot\frac{C_{ox}\cdot q_0}{2C_{si}}\Big/\left(1+\frac{q_0C_{ox}}{2C_{si}}\right)$. Also note that if i_s is denoted as the current entering the device through the source terminal we have to negate Y^q_{sd} and Y^q_{ss}. Now we derive the normalized conventional voltage domain y parameters in terms of charge based Y parameters as follows:

$$y_{d(s)x} = \frac{di_{d(s)}}{dv_x} = \frac{\partial i_{d(s)}}{\partial v_x} + \frac{\partial i_{d(s)}}{\partial q_s}\frac{\partial q_s}{\partial v_x} + \frac{\partial i_{d(s)}}{\partial q_d}\frac{\partial q_d}{\partial v_x} = 0 + Y^q_{d(s)s}\frac{\partial q_s}{\partial v_x} + Y^q_{d(s)d}\frac{\partial q_d}{\partial v_x} \tag{59}$$

The first term in (59) will always be zero because from (47) we can see that neither $\overline{i_s}$ nor $\overline{i_d}$ is an explicit function of terminal voltages. Now let us derive the four important un-normalized y parameters for DGMOS.

$$y_{d(s)g} = \frac{I_{spec}}{U_T}\left[Y^q_{d(s)s}\frac{\partial q_s}{\partial v_g} + Y^q_{d(s)d}\frac{\partial q_d}{\partial v_g}\right]$$

$$y_{sd} = \frac{I_{spec}}{U_T}\left[Y^q_{ss}\frac{\partial q_s}{\partial v_d} + Y^q_{sd}\frac{\partial q_d}{\partial v_d}\right]$$

$$y_{ds} = \frac{I_{spec}}{U_T}\left[Y^q_{ds}\frac{\partial q_s}{\partial v_s} + Y^q_{dd}\frac{\partial q_d}{\partial v_s}\right] \tag{60}$$

Substituting $v_{ch} = v_s$, v_d and $q_0 = q_s$, q_d, respectively, in (4) we obtain,

$$\frac{\partial q_{d(s)}}{\partial v_g} = \frac{1}{2 + \frac{1}{q_{d(s)}} + \frac{\frac{C_{ox}}{2C_{si}}}{1+\frac{q_{d(s)}C_{ox}}{2C_{si}}}} \tag{61}$$

and

$$\frac{\partial q_{d(s)}}{\partial v_{d(s)}} = -\frac{1}{2 + \frac{1}{q_{d(s)}} + \frac{\frac{C_{ox}}{2C_{si}}}{1+\frac{q_{d(s)}C_{ox}}{2C_{si}}}} \tag{62}$$

where $\frac{\partial q_d}{\partial v_s}$ and $\frac{\partial q_s}{\partial v_d}$ are zero

4.1. Derivation of other voltage domain y parameters

As we are dealing with symmetric DG MOSFET, we have three terminals, both the gates are tied to form a single gate terminal, and we have the source and drain terminals. So we can write the y parameter matrix as follows-

$$\begin{bmatrix} i_d \\ i_s \\ i_g \end{bmatrix} = \begin{bmatrix} y_{dg} & y_{ds} & y_{dd} \\ y_{sg} & y_{ss} & y_{sd} \\ y_{gg} & y_{gs} & y_{gd} \end{bmatrix} \begin{bmatrix} v_g \\ v_s \\ v_d \end{bmatrix} \tag{63}$$

where all symbols represent small signal quantities. Now if we keep, $v_d = v_s = 0$, and remembering that $i_d + i_s + i_g = 0$, we can show [10],

$$y_{dg} + y_{sg} + y_{gg} = 0 \tag{64}$$

Similarly we can get two more equations from the other two columns. Also, if $v_d = v_s = v_g$, there is no relative voltage drop between the terminals, so all small signal currents are zero. So we obtain [10]

$$y_{dg} + y_{ds} + y_{dd} = 0 \tag{65}$$

Similarly we get two more equations from the other two rows. Finally from these six equations we can determine all the y parameters of DG MOSFET.

4.2. Importance of the small signal model and its implementation

It is worth noting that when the cubic spline method is implemented in verilog A, both the large signal and small signal analysis can be performed due to the sub-circuit based approach followed in [21]. However, this works only for verilog A and some specific simulator interfaces. There are in-house simulators in various industries where both transient and small signal model needs to be coded separately. In addition, large signal NQS is very difficult to converge. Having a separate small signal model will help designers to explore NQS effects in their circuits in the cases where large signal NQS does not converge. Formulation in terms of Bessel functions helps us to gain a physical insight into the problem. Moreover an analytical formulation is indeed invaluable from the point of view of a circuit designer since it enables him to see how bias conditions and other device parameters change the various y parameters of the device.

Numerical evaluation of Bessel functions of fractional orders and complex arguments tends to be slow. However solutions to such problems have already been discussed in [3,4]. In [3], the authors have taken second order polynomial approximations to get a form implementable in a circuit simulator. Later in [4], an approximate NQS parameter model was presented, based on asymptotic behavior of Bessel functions. After using suitable approximations, their final form contains only sine and cosine hyperbolic terms and can easily be implemented in a circuit simulator.

5. Model validation and discussion

Two-dimensional device simulations were done on symmetrical DG MOSFET, using 2 D Atlas Device simulator [17]. The device structure was created with abrupt source and drain-body junctions. The body was kept undoped (i.e. intrinsic), and the source and drain re-

gions were kept short in length and were doped at 10^{19} cm^{-3} n-type. In order to focus on just the non-quasi-static effects, other models were disabled, such as vertical-field mobility degradation, parallel field dependent mobilty, and doping-dependent mobility. Recombination generation models, quantum mechanical models, etc., were also turned off. A constant mobility of 300 cm^2/(V s) has been used. A midgap work function metal with a zero barrier with respect to intrinsic silicon was used for the gate electrodes. The DG MOSFET has a length and width of 1 μm, oxide thickness of 1.5 nm and silicon body thickness, t_{si} of 10 nm.

5.1. Validation of the large signal NQS model

To validate the large signal model, we apply a rising and falling ramp at the gate. This results in extreme transients. The voltage waveforms applied at the gate are shown in Fig. 2. The rise time of gate voltage is 50 ps which is less than the transit time of the device. The transit time (≈66 ps) of the device is estimated as $\frac{L^2}{\mu_n \cdot (V_{gs}-V_{to})}$ where V_{to}= gate work function(=0) − U_T·ln(q_{int}/2) [6]. Next, we give the current waveforms for the four cases as mentioned below:

(1) A rising ramp applied at the gate while saturation condition is ensured.
(2) A falling ramp applied at the gate while saturation condition is ensured.
(3) A rising ramp applied at the gate while linear condition is ensured.
(4) A falling ramp applied at the gate while linear condition is ensured.

To ensure a saturation condition we have kept V_{ds} = 1 V, while for biasing the DGMOS in linear region we have kept V_{ds} = 0.1 V. As we can see, there is appreciable match between the proposed model and the results obtained from the device simulator (Figs. 3–6).

To see how the non-quasi-static model differs from the quasi-static model, we recall from (27)

$$i_d(\tau) = i_0(\tau) - \frac{d}{d\tau} \cdot \int_0^1 q_i \xi d\xi \tag{66}$$

The main assumption of the QS models is that the channel charge reaches the steady-state profile instantaneously. Using it and the fact that $L(q_i) \approx q_i^2 + 2q_i$, we get,

$$\int_0^1 q_i \xi d\xi = \int_0^1 \xi(-1 + \sqrt{1 + L(q_{is}) - \xi(L(q_{is}) - L(q_{id}))})d\xi \tag{67}$$

(67) can be used in (66) to get the expression for large signal quasi-static current in terms of $q_{is}, q_{id}, \frac{dq_{is}}{d\tau}$ (q_{is} and q_{id} represent total source and drain normalized charge) and $\frac{dq_{id}}{d\tau}$ only. The expression can be derived in a closed form, however it is too long to provide it here. When the QS current component has been obtained, it can be subtracted from the total current derived in (29) to obtain the non-quasi-static component alone. Various components of drain current, i.e. $i_0(t)$ (computed from the DC equation with time varying voltages), quasi-static, non-quasi-static (=total − quasi-static) and total drain current, $i_d(t)$ are shown in Fig. 7. The drain voltage is kept at 1 V and gate is ramped from 0 to 1 V. Ramp time is 50 ps, from 30.303 ps to 80.303 ps. During the process $q_{id} \approx 0$, but q_{is} increases

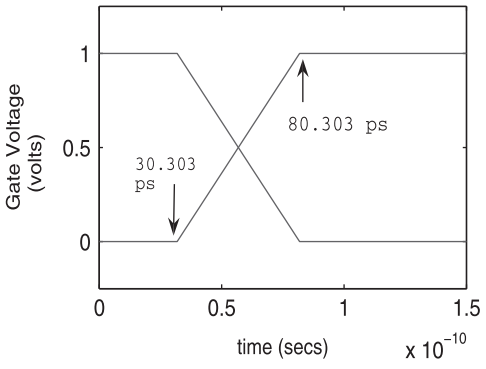

Fig. 2. The rising and falling gate voltage waveforms.

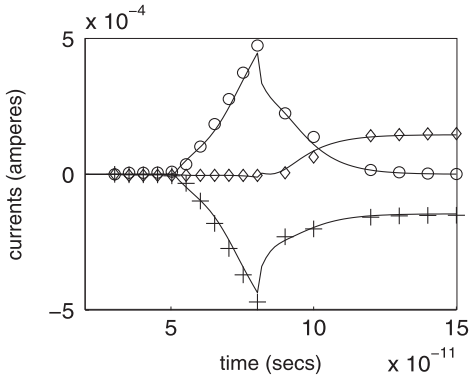

Fig. 3. Various currents when a rising ramp is applied at the gate in saturation: continuous lines represent model and symbols represent device simulation results. Diamond, '+' and 'o', respectively, stand for drain, source and gate current.

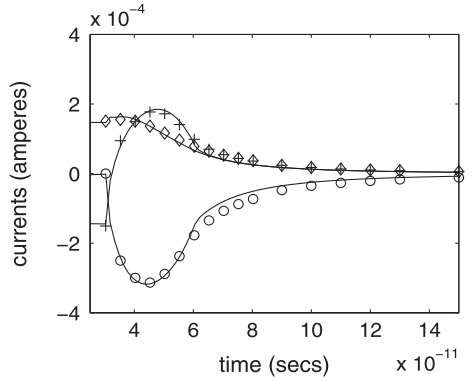

Fig. 4. Various currents when a falling ramp is applied at the gate in saturation: continuous lines represent model and symbols represent device simulation results. Diamond, '+' and 'o', respectively, stand for drain, source and gate current.

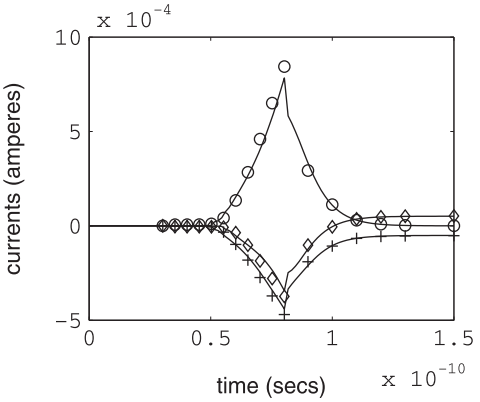

Fig. 5. Various currents when a rising ramp is applied at the gate in linear region: continuous lines represent model and symbols represent device simulation results. Diamond, '+' and 'o', respectively, stand for drain, source and gate current.

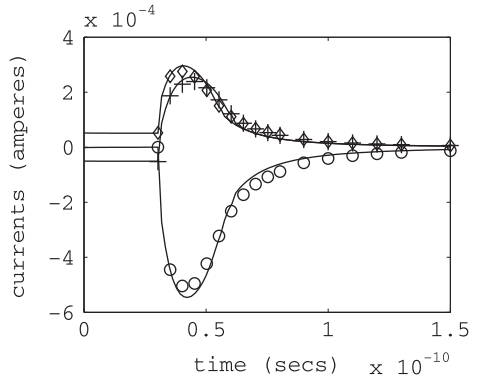

Fig. 6. Various currents when a falling ramp is applied at the gate in linear region: continuous lines represent model and symbols represent device simulation results. Diamond, '+' and 'o', respectively, stand for drain, source, and gate current.

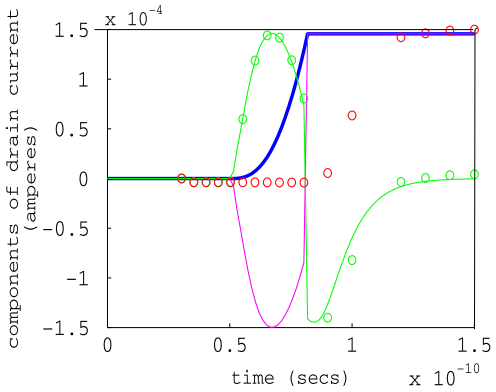

Fig. 7. Various components of drain current when a rising ramp is applied at the gate in saturation region: lines represent model and symbols represent device simulation results. Red, magenta, green and blue, respectively, stand for total, quasi-static, $i_0(t)$, and NQS component of drain current.

as gate voltage inceases, hence $\frac{dq_{is}}{dt} > 0$. The quasi-static component of the current is negative during the rise time of gate voltage. The difference between the QS charge and the actual charge only increases during the rise time of the ramp. However the total drain current is still zero because the electron wavefront has still not arrived at the drain. So the NQS component is positive and is equal to the magnitude of the quasi-static component. We also notice that there is a small, almost flat portion in the non-quasi-static component (green[2] curve, see the most negative part of the curve) between the time when $i_0(t)$ has reached its steady-state value (as gate voltage has reached the steady-state value of 1 V) and the total drain current actually starts to build up. It is because of the fact that before the transit time, $i_d(t)$ is zero and the quasi-static current has reached the value $i_0(t)$ as $\frac{dq_{is}}{d\tau} = \frac{dq_{id}}{d\tau} = 0$. So, the NQS component of the drain current is equal to the negative of the QS component and also, it is invariant with time. If the transit time is more, this flat portion of the curve is elongated. Finally, after the charge profile reaches the drain, $i_d(t)$ starts to flow and non-quasi-static component of the current gradually goes to zero.

5.2. Validation of the small-signal NQS model

5.2.1. Operation in saturation region

We keep $V_{ds} = V_{gs} = 1$ V to ensure saturation condition. A comparison of device simulations and our model, is shown in Figs. 8–11. We see that our model gives good results upto 50 GHz, which is 14 times the cut off frequency (3.5368 GHz), calculated as $\frac{g_m}{2\cdot\pi\cdot C_{gg}}$, where g_m and C_{gg} are obtained from atlas simulations [17] at $V_d = V_g = 1$ V. In saturation, the drain charge q_d is zero, so the second terms in (60) are zero. So only the first terms contribute in saturation. We are neglecting velocity saturation and channel length modulation which results into non-zero drain charge and hence the second terms in (60) will not be zero anymore. Let us first consider the variation of y_{dg} with frequency. In saturation only Y^q_{ds} contributes to y_{dg}. Y^q_{ds} essentially represents the variation in the small signal drain current with a perturbation in the source charge. The behavior of Y^q_{ds} with frequency is illustrated in Fig. 12, where we

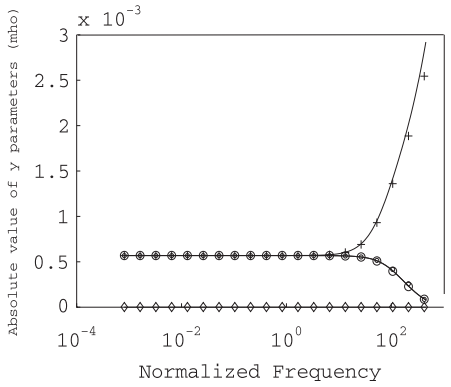

Fig. 8. Magnitude of y parameters versus frequency in saturation, '+' stands for y_{sg}, 'o' for y_{ds} and y_{dg}, diamond sign for y_{sd}. Continuous lines represent model and symbols represent device simulations. y_{ds} and y_{dg} superimpose. Normalized DC current $i_0 = 79$.

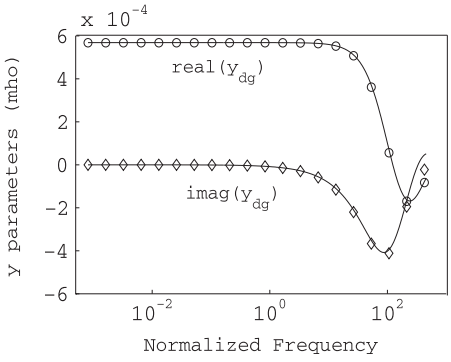

Fig. 9. y_{dg} versus frequency at $V_{ds} = 1$ V, $V_{gs} = 1$ V, normalized drain current $i_0 = 79$.

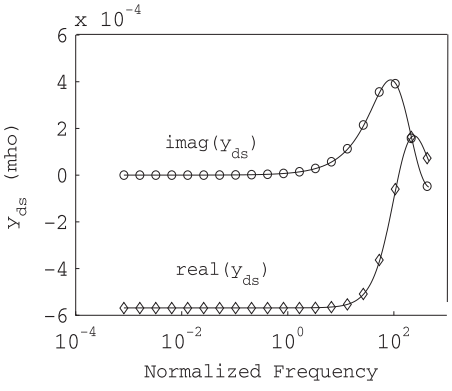

Fig. 10. y_{ds} versus frequency at $V_{ds} = 1$ V, $V_{gs} = 1$ V.

[2] For interpretation of color in Figs. 1 and 7, the reader is referred to the web version of this article.

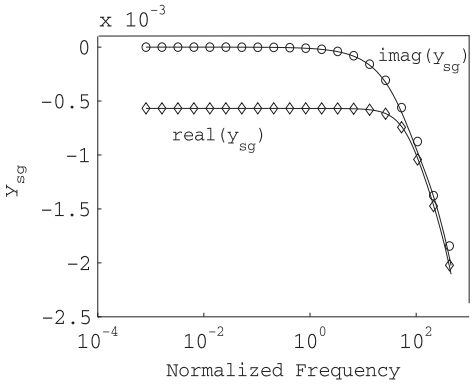

Fig. 11. y_{sg} versus frequency at $V_{ds} = 1$ V, $V_{gs} = 1$ V.

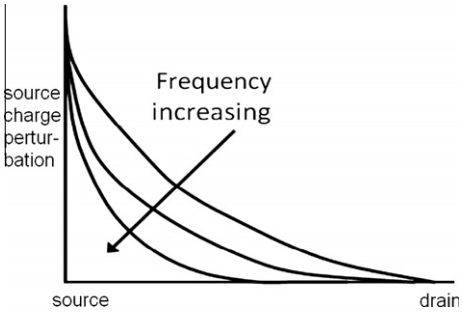

Fig. 12. Illustration of high frequency behavior of Y^q_{ss} and Y^q_{ds}: a perturbed charge profile when the perturbation is at the source.

see that if a charge perturbation is applied at the source, its contribution at the drain decreases with increase in frequency because of very small slope of the profile at the drain. Therefore y_{dg} continuously decreases with frequency. For y_{ds}, the same explanation goes, infact magnitude of y_{ds} is same as magnitude of y_{dg} which is evident from (60)–(62). From (60) it is clear that $y_{sd} \approx 0$ in saturation because $\frac{\partial q_s}{\partial v_d}$ and $\frac{\partial q_d}{\partial v_d}$ both are zero. In saturation y_{sg} is governed by Y^q_{ss}. It essentially means the variation in the source small signal current with a charge perturbation at the source. As frequency increases, the slope of the charge profile at the source increases (Fig. 12), hence Y^q_{ss} increases,leading to increase in magnitude of y_{sg} with frequency. Also note that, $y_{sg} + y_{dg} + y_{gg} = 0$. At low frequencies, $y_{gg} \approx 0$, hence $y_{sg} \approx -y_{dg}$. That is evident from Fig. 8

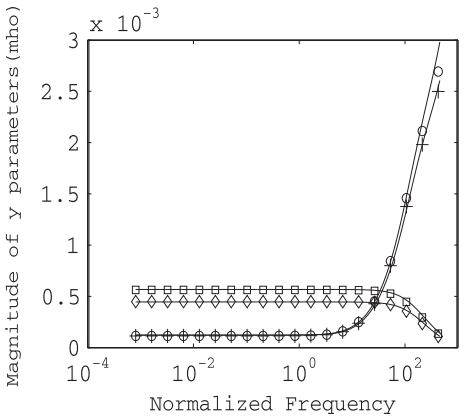

Fig. 13. Magnitude of y parameters versus frequency in linear region, 'o' for y_{sg}, '+' for y_{dg}, squares for y_{ds}, and diamonds for y_{sd}. Continuous lines represent model and symbols represent device simulations. Normalized current, $i_0 = 27.6$.

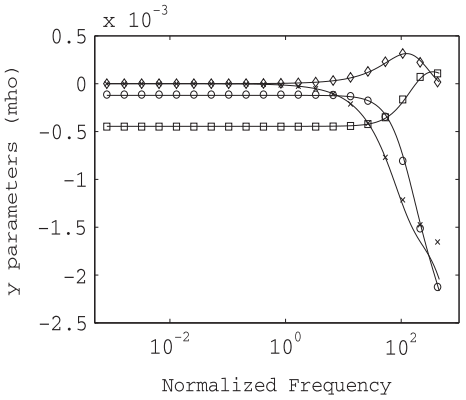

Fig. 14. y_{sg} and y_{sd} versus frequency in linear region, 'x' for imag(y_{sg}), 'o' for real (y_{sg}), diamond for imag(y_{sd}), square for real (y_{sd}).

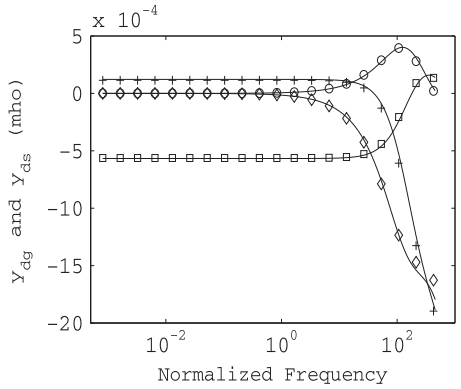

Fig. 15. y_{dg} and y_{ds} versus frequency in linear region. '+' Represents real (y_{dg}), diamond for imag (y_{dg}), 'o' for imag(y_{ds}), squares for real (y_{ds}).

5.2.2. Operation in linear region

We keep $V_{gs} = 1$ V and $V_{ds} = 0.1$ V to bias it in linear (conduction) mode. A comparison of device simulations and our model, is shown in Fig. 13–15. Now as the device is biased in linear region $q_d \neq 0$ and so the second terms in (60) are no more zero. So now all the charge based Y parameters i.e. $Y^q_{ds}, Y^q_{ss}, Y^q_{sd}, Y^q_{dd}$ contribute.

The first thing we note is that magnitude of y_{ds} and y_{dg} are no longer equal , it is because of non-zero y_{dd} [see (65)] (or equivalently finite channel resistance). $y_{sg} \approx -y_{dg}$ at low frequencies is valid in linear region also. From the discussion we already had, we can say that Y^q_{ss}, Y^q_{dd} increases with frequency and Y^q_{sd}, Y^q_{ds} decreases with frequency. y_{dg} and y_{sg} have, respectively, Y^q_{dd} and Y^q_{ss} contributing to their increase with frequency, whereas y_{ds} and y_{sd} has contribution from Y^q_{ds} and Y^q_{sd}, respectively, so they fall with frequency. Also we see that $y_{sd} \approx y_{ds}$ and $y_{dg} \approx y_{sg}$ from Fig. 14 and 15, this emphasizes the interchangeability of the source and drain terminals.

6. Conclusion

In this paper, we derived a unified model for large signal and small-signal NQS parameters of symmetric double gate MOSFETs using charge-based modeling approach that is valid in all regions of inversion. The model has been seen to be in good agreement with 2D simulations. It has also been demonstrated that only four complex transadmittances are needed to fully characterize the small signal operation of the device and all other transadmittance parameters can be deduced from them. Most parameters in the model are expressed in terms of normalized variables, which are independent of the process parameters.

Acknowledgement

One of the authors, Sudipta Sarkar would like to thank Rutwick Kumar Kashyap, Nanoscale Device Research Lab, CEDT, Indian Institute of Science for discussions on spice and implementation issues of the proposed models.

References

[1] Sarkar Sudipta, Roy Ananda S, Mahapatra Santanu. A non-quasi-static small signal model for long channel symmetric DG MOSFET. Proc Int Conf VLSI Des 2010:21–6.
[2] Roy Ananda S, Enz Christian C, Sallese Jean-Michel. Compact modeling of anomalous high-frequency behavior of MOSFET's small-signal NQS parameters in presence of velocity saturation. IEEE Trans Electron Dev 2006;53(9):2044–50.
[3] Sallese JM, Porret A-S. A novel approach to charge-based non-quasi-static model of the MOS transistor valid in all modes of operation. Solid-State Electron 2000;44:887–94.
[4] Porret AS, Sallese JM, Enz CC. A compact non-quasi-static extension of a charge-based MOS model. IEEE Trans Electron Dev 2001;48(8):1647–54.
[5] Lu Huaxin, Taur Yuan. An analytic potential model for symmetric and asymmetric DG MOSFETs. IEEE Trans Electron Dev 2006;53(5):107–9.
[6] Diagne Birahim, Pre'galdiny Fabien, Lallement Christophe, Sallese Jean-Michel, Krummenacher Francois. Explicit compact model for symmetric double-gate MOSFETs including solutions for small-geometry effects. Solid-State Electron 2008;52:99–106.
[7] Pregaldiny F, Krummenacher F, Sallese J-M, Diagne B, Lallement C. An explicit quasi-static charge-based compact model for symmetric DG MOSFET NSTI-Nanotech; 2006.
[8] Lu Huaxin, Yu Bo, Taur Yuan. A unified charge model for symmetric double-gate and surrounding-gate MOSFETs. Solid-State Electron 2008;52:67–72.
[9] Borli Hakon, Kolberg Sigbjorn, Fjeldly Tor A. Capacitance modeling of short-channel double-gate MOSFETs. Solid-State Electron 2008;52:1486–90.
[10] Tsividis Y. Operation and modeling of the MOS transistor. 2nd ed. New York: Oxford university press; 2003.
[11] Chan M, Hui KY, Hu C, Ko PK. A robust and physical BSIM3 non-quasi-static transient and AC small-signal model for circuit simulation. IEEE Trans Electron Dev 1998;45(4):834–41.
[12] Scholten AJ, Tiemeijer LF, de Vreede PWH, Klaassen DBM. A large signal non-quasi-static MOS model for RF circuit simulation. EDM Tech Dig 1999:163–6.
[13] Roy Ananda S, Vasi Juzer M, Patil Mahesh B. A new approach to model nonquasi-static (NQS) effects for mosfets-part i: large-signal analysis. IEEE Trans Electron Dev 2003;50(12):2393–400.
[14] Wang Hailing, Chen Ten-Lon, Gildenblat Gennady. Quasi-static and nonquasi-static compact MOSFET models based on symmetric linearization of the bulk and inversion charges. IEEE Trans Electron Dev 2003;50(11):2262–72.
[15] Wang H, Gildenblat G. A robust large signal non-quasi-static MOSFET model for circuit simulation. In: IEEE custom international circuits conference; 2004.
[16] Sallese Jean-Michel, Krummenacher Francois, Prégaldiny Fabien, Lallement Christophe, Roy A, Enz C. A design oriented charge-based current model for symmetric DG MOSFET and its correlation with the EKV formalism. Solid-State Electron 2005;49:485–9.
[17] Atlas User's Manual, version Y.2008.06.
[18] Enz Christian C, Vittoz Eric A. Charge based MOS transistor modeling. West Sussex (England): Wiley; 2006.
[19] Prégaldiny F, Krummenacher F, Diagne B, Pecheux F, Sallese J-M, Lallement C. Explicit modelling of the double-gate MOSFET with VHDL-AMS. Int J Numer Model: Elec Network Dev Fields 2006;19(3):239–56.
[20] Oh Soo-Young, Ward Donald E, Dutton Robert W. Transient analysis of MOS transistors. IEEE J Solid State Circ 1980;15(4):636–49.
[21] Wang H, Li X, Wu W, Gildenblat G, van Langevelde R, Smit GDJ, et al. A unified nonquasi-static MOSFET model for large-signal and small-signal simulations. IEEE Trans Electron Dev 2006;53(9):2035–43.